Combustion Theory and Modelling
Vol. 16, No. 4, 2012, 650–678

Taylor & Francis
Taylor & Francis Group

Effects of high activation energies on acoustic timescale detonation initiation

J.D. Regele[a], D.R. Kassoy[b] and O.V. Vasilyev[b]*

[a]*California Institute of Technology, Pasadena, CA 91125, USA;* [b]*University of Colorado, Boulder, CO 80309, USA*

(*Received 31 March 2011; final version received 7 October 2011*)

Acoustic timescale Deflagration-to-Detonation Transition (DDT) has been shown to occur through the generation of compression waves emitted by a hot spot or reaction centre where the pressure and temperature increase with little diminution of density. In order to compensate for the multi-scale nature of the physico-chemical processes, previous numerical simulations in this area have been limited to relatively small activation energies. In this work, a computational study investigates the effect of increased activation energy on the time required to form a detonation wave and the change in behaviour of each hot spot as the activation energy is increased. The simulations use a localised spatially distributed thermal power deposition of limited duration into a finite volume of reactive gas to facilitate DDT. The Adaptive Wavelet-Collocation Method is used to solve efficiently the 1-D reactive Euler equations with one-step Arrhenius kinetics. The DDT process as described in previous work is characterised by the formation of hot spots during an initial transient period, explosion of the hot spots and creation of an accelerating reaction front that reaches the lead shock and forms an overdriven detonation wave. Current results indicate that as the activation energy is raised the chemical heat release becomes more temporally distributed. Hot spots that produce an accelerating reaction front with low activation energies change behaviour with increased activation energy so that no accelerating reaction front is created. An acoustic timescale ratio is defined that characterises the change in behaviour of each hot spot.

Keywords: detonation initiation; deflagration-to-detonation transition; acoustic timescale; inertial confinement; wavelets

1. Introduction

Thermal energy deposition into a reactive gas provides an ignition source for detonations. Sufficiently fast and large energy addition can facilitate a direct initiation. Clarke, Kassoy and Riley [1] and Clarke, Kassoy, Meharzi, Riley and Vasantha [2] model detonation initiation following localised spatially distributed transient energy deposition from a planar boundary via conduction into an adjacent reactive gas in a semi-infinite domain. The Navier–Stokes equations are integrated numerically to resolve a quantitative time-history of localised spatially distributed reactive gasdynamic processes that lead to planar detonation formation. The authors recognise that '. . . direct initiation of detonation requires sufficient power input to first of all generate a suitably strong precursor shock wave, which then becomes the trigger to switch on vigorous chemical activity in its wake. The hall mark of

*Corresponding author. Email: oleg.vasilyev@colorado.edu

ISSN: 1364-7830 print / 1741-3559 online

http://dx.doi.org/10.1080/13647830.2011.647090
http://www.tandfonline.com

this vigour is its capacity to exploit the inertia of the fluid by raising local pressures and temperatures, with little diminution in local density; the pressure waves so formed propagate and increase precursor shock strength which therefore lifts the overall density levels, as well as those of pressure and temperature. All of these processes interlock in a continuously accelerated sequence that progresses towards a steady-state. . . ZND detonation' [1].

Subsequently, Mazaheri [3] and Eckett, Quirk and Shepherd [4, 5], model planar and spherical detonation initiation, respectively, initiated by blast waves subsequent to instantaneous deposition of energy at a plane or a point. Energy deposition criteria are used to distinguish between sustained and failed detonations. Computational modelling results demonstrate that blast wave propagation through unreacted gas mixture leads to the formation of localised regions of rapid chemical heat release (thermal explosions) characterised by relatively high temperature and pressure, similar to those found in [1] and [2]. These hot spots are the subsequent sources of compression waves that may run up to and strengthen the blast wave front enough to generate and sustain a classical detonation (shock coupled to a reaction zone).

Sileem, Kassoy and Hayashi [6] (SKH) and Kassoy *et al.* [7, 8] (KKNC), model the reactive gas response to relatively smaller spatially distributed, transient energy deposition into a finite target volume.[1] They describe the sequence of reactive gasdynamic events occurring beyond the initially heated volume that are classified as DDTs. Computational results, based on MacCormack numerical methods with fixed grids, demonstrate that hot spots are inherent to the detonation initiation process.

Gu, Emerson and Bradely [9] use computational solutions to the Euler equations with multistep kinetics relevant to H_2–CO–air and H_2–air mixtures to identify five distinct modes of reaction front propagation arising from a preexisting local hot spot. They find that evolution of the detonative mode depends on the temperature distribution properties of the hot spot AND '. . . the ratio of the hot spot acoustic time to the heat release rate excitation time. . . ' [9].

Hot spots appear to be common to all forms of detonation initiation studies, including those associated with reflected shocks and shock flame interactions studied intensively by Oran and co-workers beginning in the 1980s ([10–14] and reviewed by Oran and Gamezo [15]). Nearly all studies of detonation initiation contain qualitative descriptions of the role played by hot spots in the development of detonations. Since the early experimental observation by Oppenheim [16] of an 'explosion in an explosion' (reaction centre) it has been argued qualitatively that hot spots are local sources of compression waves that strengthen existing lead shocks to promote the existence of coupled reaction zones. That argument depends on the simultaneous local increase in temperature and pressure caused by localised chemical heat release in a nearly inertially confined fluid volume (constant volume heating) characterised by a minimal change in density as recognised in [1].

Zeldovich *et al.* [17], Zeldovich [18] and Lee [19] proposed concepts to quantify how hot spots contribute to the formation of detonations. Both concepts depend on a spatial gradient in chemical induction time $\tau(\boldsymbol{r})$ where a reaction forms at the minimum induction location and a spontaneous reaction wave propagates at a speed equal to the inverse gradient of the induction scalar field $u_{\rm sp} = |\nabla\tau(\boldsymbol{r})|^{-1}$. As an alternative to the Zeldovich [17] and Lee (SWACER) [19] models, Bauwens [20, 21] developed a 1-D alternative theory that

[1] Extensive discussions of both direct initiation of detonations and Deflagration-to-Detonation Transition (DDT), including references, are found in all of the aforementioned publications.

focuses on the chemical and gasdynamic timescales of shocks and expansion waves to create detonability limits for one or a series of hot spots.

Hot spot modelling, based on spatially distributed Thermal Explosion Theory (TET), has been developed with a combination of asymptotic and computational methodologies (e.g. Jackson, Kapila and Stewart [22], Short [23,24]). Results describe spatially distributed, transient chemical heat release during a relatively lengthy induction period, followed by a much shorter period of extremely rapid energy deposition (the explosion) into a relatively tiny spatial volume. These hot spot theories describe the thermomechanical properties of the chemically heated gas, but are not formulated to consider the subsequent impact of focused rapid heat release on environmental gases.

Vasquez-Espi and Linan [25] formulate a model for non-diffusive ignition of a gaseous reacting mixture subject to a point energy source. Their intuitive analysis identifies the thermodynamic response of the gas-to-source heating. The fluid motion induced by spatially distributed transient energy addition, observed in many related studies (e.g. [1–9]) is not calculated. Gas expansion subsequent to thermal energy addition is shown to be a significant cooling mechanism that may suppress any anticipated spatially distributed thermal explosion or lead to diffusive ignition.

An initial step toward developing a completely rational parameter-based asymptotic thermomechanical study of hot spots has been developed by Kassoy [26]. An external source provides spatially distributed transient heat addition to a finite volume of inert gas on a timescale short compared to the acoustic time of the volume where the ratio is represented by the parameter ε. The theory defines limits on energy addition compatible with near inertially confined heat addition within the targeted volume (nearly constant volume heating in the near field) characterised by a synchronised increase in spatially distributed temperature and pressure with only small changes in density. The internal expansion Mach number will be asymptotically small with respect to the parameter ε when the energy addition is sufficiently small during the heating time period. Hot gas expelled from the volume (the piston effect) during the heating process generates only acoustics in the neighbouring cold gas (the far field). Alternatively, for sufficiently large energy addition, more 'robust' piston Mach numbers are predicted leading to immediate shock propagation in the far field. When the energy addition reaches a specific maximum value the near field heating process is entirely compressible, characterised by localised hypersonic expansion Mach numbers, compatible with very strong blast wave generation in the far field.

Although it is tangential to the current work, it should be noted that hot spots are also of interest in homogeneous charge compression ignition (HCCI) engine modelling (Sankaran *et al.* [27]). 'High fidelity' simulations are performed to identify autoignition processes in turbulent, high-pressure homogeneous H_2–air mixtures with localised temperature distributions. Two distinct ignition regimes are identified: spontaneous propagation and deflagration. Here the objective is to avoid detonation initiation and the presence of shock waves.

Clarke *et al.* [1,2], Sileem, Kassoy and Hayashi [6] and Kassoy *et al.* [7,8] perform 1-D numerical simulations based on the reactive Euler equations whereby DDT is initiated by depositing energy into a finite volume of reactive fluid of size l' for a finite duration t'_{h} such that the fluid response is characterised by some degree of inertial confinement if $t'_{\mathrm{h}} \ll t'_{\mathrm{a}}$ or $t'_{\mathrm{h}} \lesssim t'_{\mathrm{a}}$, where the acoustic timescale $t'_{\mathrm{a}} = l'/a'$ is defined by the fluid dimension and the local speed of sound. The simulations demonstrate that if $t'_{\mathrm{h}} \sim t'_{\mathrm{a}}$ a chemical explosion occurs in the deposition region, leading to the formation of compression waves that become shock waves. The shocks decouple from the reaction zone and an induction zone is formed

between the reacted volume of fluid and the lead shock that conditions the reactive gas. After a period of time, a localised explosion occurs inside of the induction zone. In [6], the localised explosion occurs when a hot spot releases chemical heat rapidly. Hot spots are observed to form behind a strong lead shock created by the coalescence of two relatively weak shocks, similar to the experimental observations in Oppenheim [28]. Coalescence of two shocks initiates the rapid localised reaction process leading to a sequence of events resulting in an overdriven detonation. Transition to detonation is conditional upon creating a sufficiently strong lead shock, which provides the temperature rise required for adequate chemical heat addition.

In [8], similar trends are observed while exploring the effects of a narrow range of nondimensional activation energies (13.79, 13.33, 12.90 and 12.50) and variations in local power deposition rates. Smaller activation energy is associated with relatively shorter times to detonation formation. However, the basic characteristics of global heat release profiles (spatially integrated chemical heat release at each instant of time) are similar. Each shows evidence of discrete localised hot spot formation and evolution. In [8], the authors also explore the effects of decreasing the power deposition rate up to 50% of the initial value. As the rate is decreased the time to form a detonation increases. The global heat release profiles exhibit a definitive change in behaviour, especially in the case of 50% power. In this case the global heat release plot suggests that the sequence of hot spots evolves with time creating multiple peaks in the global heat release rate. The authors conclude that the induction zone time increases as a result of a decrease in induction zone temperature. No explanation is offered for the appearance of a sequence of heat release maxima. A point worth noting, although not formally concluded by the authors, is that increased power deposition is shown to reduce the number of heat release maxima.

The previous studies by Kassoy and co-workers [6, 8] are based on the reactive Euler equations. A 1-D uniform grid is used in a MacCormack scheme. Proper resolution of a detonation half-reaction length requires a minimum of 50 or more points [29–31]. Since the previous work used uniform grid serial based solvers involving computational limitations, relatively small nondimensional activation energies $E \in [10, 13.78]$ (see Table 1) were employed. This is effectively done by reducing the multi-scale nature of the thermomechanical behaviour such that the size of the localised hot spots is within an order of magnitude of the computational domain and the timescale associated with the chemical heat release of the hot spots is approximately within an order of magnitude of the total time to form a detonation. However, activation energies typical of hydrocarbon–air mixtures are approximately in the range 25–50 and other large-scale simulations [15] and experiments [28] demonstrate the full multi-scale nature of these thermomechanical processes. Although these examples contain multi-dimensional effects, it is still reasonable to question whether the initiation sequence description observed for relatively small activation energies will prevail when higher, more realistic values are employed.

The multi-scale nature of acoustic timescale detonation initiation requires more advanced numerical integration schemes that use dynamically changing grids. The dynamically Adaptive Wavelet-Collocation Method (AWCM) has been shown to use computational resources efficiently for simulations that involve localised structures [32–34], such as those found in the detonation initiation process. The efficiency of the AWCM arises from the use of wavelets to determine which grid points to use during each time step, based upon a given error threshold parameter ϵ. A hyperbolic solver has been developed specifically for the AWCM [35, 36] and efficiently captures shocks, contacts and material interfaces by maintaining a Total Variation Diminishing (TVD) solution through the use of artificial viscosity. With this numerical algorithm, it is possible to capture the multi-scale phenomena

inherent with larger activation energies. The one-dimensional results presented in this work appear in a PhD thesis [36] also containing two-dimensional results [37]. The latter are to be described in more detail in a forthcoming manuscript.

There are five primary objectives in this work. The first is to confirm qualitative conceptual ideas about DDTs obtained originally from computational results based on MacCormack methods with results obtained from AWCM computations. Second, to explore the sensitivity of the evolutionary process to relatively small increases in activation energy beyond that done in [8]. Third, to demonstrate the truly multi-scale behaviour observed with more realistic activation energies and explain how the difference in behaviour occurs. Fourth, to identify the importance of full or partial inertial confinement in the evolution of 1-D hot spots. Finally, to explain the thermomechanical response of the reactive gas in terms of concepts developed by Kassoy [26].

2. Mathematical model

The nondimensional 1-D reactive Euler equations (see Table 1 for variable definitions) are used to model detonation initiation. They are written in terms of the conserved quantities ρ, ρu, the total energy ρe_{T} and the reactant mass ρY:

$$\frac{\partial \rho}{\partial t} + \frac{\partial \rho u}{\partial x} = 0, \tag{1a}$$

$$\frac{\partial \rho u}{\partial t} + \frac{\partial}{\partial x}(\rho u^2 + p) = 0, \tag{1b}$$

$$\frac{\partial \rho e_T}{\partial t} + \frac{\partial}{\partial x}(\rho e_{\mathrm{T}} + p)u = \dot{Q} + \dot{W}q, \tag{1c}$$

$$\frac{\partial \rho Y}{\partial t} + \frac{\partial \rho Y u}{\partial x} = -\dot{W}. \tag{1d}$$

The equation of state and reaction rate are defined by

$$p = (\gamma - 1)\left(\rho e_{\mathrm{T}} - \frac{1}{2}\rho u^2\right), \tag{2}$$

$$\dot{W} = B\rho Y \exp(-E/T), \tag{3}$$

Table 1. Nondimensional variable definitions (primes denote dimensional quantities).

Position	$x = x'/l'$
Time	$t = t'/t'_a$
Velocity	$u = u'/a'_o$
Pressure	$p = p'/\gamma p'_o$
Density	$\rho = \rho'/\rho'_o$
Temperature	$T = T'/T'_o$
Total Energy	$e_{\mathrm{T}} = e'_{\mathrm{T}}/a'^2_o$
Activation energy	$E = E'/R'T'_o$
Heat of reaction	$q = q'/a'^2_o$
External power deposition	$\dot{Q} = \dot{Q}'t'_a/\rho'_o a'^2_o$
Pre-exponential factor	$B = B't'_A$

where Y is the mass fraction of the reactants, q is the heat of reaction and $\dot{Q}$ is an externally added power addition term. The reaction rate $\dot{W}$ represents an Arrhenius reaction rate where B is the pre-exponential factor, E is the activation energy and $T = \gamma p/\rho$.

The nondimensional variables are defined in Table 1 where the thermodynamic variables (p, ρ, T) are expressed with respect to the undisturbed dimensioned initial state (p'_o, ρ'_o, T'_o) and primes indicate a dimensioned quantity. The spatial variable x is defined with respect to a characteristic length l' in the undisturbed fluid such that the acoustic timescale $t'_a = l'/a'_o$, where $a'^2_o = \gamma R' T'_o$.

3. Numerical method

Since detonation initiation is a multi-scale process, a uniform-grid based scheme may be incapable of resolving all physically important scales without intense utilisation of computational resources. For this study the dynamically Adaptive Wavelet-Collocation Method (AWCM) is used to perform the simulations [32–34]. The AWCM utilises second-generation wavelets with an error thresholding parameter ϵ to determine which grid points to use during each timestep in the solution of a partial differential equation while maintaining a prescribed level of accuracy. The hyperbolic solver [35,36] developed for the AWCM uses wavelets on the finest level of resolution to create a shock locator function $\phi \in [0, 1]$, which explicitly applies artificial viscosity to resolve shocks and contact discontinuities so that spurious oscillations in the solution are minimised. With this definition, a locator function with a value of zero indicates a smooth solution and a locator value of unity indicates a strong gradient in the solution such as a shock. It varies continuously from 0 to 1 based upon the smoothness of the solution. Further details can be found in [35]. The locator function ϕ is used in this work to track localised maxima and minima such as reaction centres or hot spots. The differencing technique is centred and is capable of using any arbitrary order of accuracy. For the simulations presented in this work the central differencing scheme is 4th-order accurate. In regions near near localised structures such as shocks and contact discontinuities, the artificial viscosity limits the accuracy in these regions to between 1st- and 4th-order accuracy.

Since previous investigations [6, 8] used a MacCormack scheme, it is anticipated that there will be quantitative differences between previous results and those presented in Section 3.1.1. Differences are expected to exist because each scheme uses different amounts of artificial viscosity near shocks and contact discontinuities. The artificial viscosity acts as a diffusion mechanism. When it is combined with an Arrhenius reaction, the reaction and heat release rates may differ between methods. The quantitative differences are most apparent in the globally integrated heat release plots. The quantitative results identified in Section 3.1.1 imply that the DDT scenarios described in [6, 8] are conceptually valid and qualitatively correct.

Since the detonation initiation transients are of primary interest and the length scales are as much as an order of magnitude larger than the reaction region, approximately 25 points are used to resolve the steady-state half-reaction length. Consequently, the globally integrated chemical heat release at each timestep can be oscillatory when a detonation eventually forms. This has been observed before in previous work [6] and it has been shown that increased resolution reduces the magnitude of these oscillations, but does not change the initiation process. A convergence study has also been performed to ensure that the results presented in this work are independent of resolution.

3.1. *Validation*

Prior to the current work, the AWCM-hyperbolic solver combination has never been applied to compressible reacting flows. In addition, the results in [6] and [8] have never been verified by comparison with those obtained from other methods. Therefore, it is important to establish a numerical starting point that ensures continuity between the past and present simulation techniques. The purpose of this section is to demonstrate the ability of the AWCM to capture compressible reacting flow and to confirm the conceptual perspectives developed in earlier papers are not dependent upon the numerical method.

In order to confirm the concepts developed in earlier work are independent of the numerical method a replica of the 1-D detonation initiation simulation with $z_i = 3$ in [8] is performed using the AWCM. First, it is necessary to demonstrate that the numerical method correctly captures the steady-state detonation propagation velocity and to understand the level of resolution required to resolve the von Neumann spike. A numerical simulation is performed with the Zeldovich–Neumann–Döring (ZND) model [38–40] solution as the initial condition. The detonation propagation velocity obtained from the numerical method is found to be nearly identical to the theoretical value and is independent of resolution. Approximately 100 points are needed to resolve the half-reaction length so that the density reduction at the von Neumann spike is less than 2% of the theoretical value. However, the pressure and temperature at the von Neumann spike are accurately captured using as little as 22 points. A detailed discussion of this validation problem can be found in Appendix A. These results indicate that the method is capable of accurately modelling compressible reacting flows.

3.1.1. *Time history evolution to detonation initiation benchmark*

Before attempting to add to the conceptual discoveries made in [6,8], it is best to confirm that the results in the previous work are not dependent upon the numerical method. This is done by replicating a simulation performed in [8]. Differences are expected to be present between the two schemes, but the underlying concepts describing the DDT process should remain consistent. The purpose of this step is to identify the differences between schemes and demonstrate that the concepts developed in [6,8] are independent of the applied numerical method.

The simulation performed is case ($z_i = 3$) in [8]. The 1-D problem is set up using the reactive Euler equations (1), the equation of state (2), the reaction rate equation (3) and an equation for the spatially resolved, transient thermal power deposition $\dot{Q}$:

$$\dot{Q} = \begin{cases} 0 & 0 \le x \le 1 \\ 3f(t)\cos\left[\dfrac{\pi}{4}(3-x)\right] & 1 < x \le 5 \\ 0 & x > 5 \end{cases} \tag{4}$$

$$f(t) = 0.7A\{\tanh[5(t-t_a)] - \tanh[5(t-t_b)]\}. \tag{5}$$

The parameters t_a and t_b are chosen to ensure rise and fall-off times of about 0.5 acoustic times while the power deposition is sustained for a much longer time. For this simulation $t_a = 0.5$ and $t_b = 10$ and the amplitude term $A = 1$. The heat of reaction $q = 15$, specific heat ratio $\gamma = 1.4$, pre-exponential factor $B = 15$ and activation energy $E = 13.79$. Equation (4) describes the power deposited in the region $x \in [1, 5]$. An adiabatic reflecting wall is located at $x = 0$. The simulation begins with the reactive gas at rest in thermal

Table 2. Dimensional values for acoustic time, pre-exponential factor, power addition rate and energy addition per unit area A' are presented for various different length scales.

Length scale l' [m]	Acoustic timescale $t'_a = l'/a'_o$ [s]	Pre-exponential $B' = B/t'_a$ [1/s]	Power addition $\dot{Q}'/\rho'_o = \dot{Q}a'^2_o/t'_a$ [W/kg]	Energy addition $Q'/A' = \dot{Q}'l't'_h$ [J/m^2]
1	2.9E−3	5.21E+3	1.76E+8	1.92E+7
10^{-1}	2.9E−4	5.21E+4	1.76E+9	1.92E+6
10^{-2}	2.9E−5	5.21E+5	1.76E+10	1.92E+5
10^{-3}	2.9E−6	5.21E+6	1.76E+11	1.92E+4
10^{-6}	2.9E−9	5.21E+9		

equilibrium with initial condition

$$\rho_o = T_o = Y_o = 1 \quad u_o = 0. \tag{6}$$

To add context to these nondimensional values, an example of a dimensional initial condition could be

$$T'_o = 300\,\mathrm{K} \quad \rho'_o = 1.16\,\mathrm{kg\,m^{-3}} \quad p'_o = 1\,\mathrm{bar} \tag{7}$$

with nondimensional parameters $B = 15$ (see Equation 5), a total heating time $t_h = t'_h/t'_a = 9.5$ and a speed of sound $a'_o = 347.2\ \mathrm{m\,s^{-1}}$. The peak nondimensional power deposition rate for an amplitude $A = 1$ is $\dot{Q} = 4.2$. Table 2 lists dimensional values of the acoustic time t'_a, the pre-exponential factor B', the power/mass deposition amplitude $\dot{Q}'/\rho'_o$ and the energy deposition per unit area into a slab of width $4l'$ during a period of $t'_h = 9.5t'_a$, as functions of the length scale l' in the range 1 m to 1 μm. These numbers provide some perspective on the dimensional time and space scales incorporated by the model, as well as the power and energy deposition levels used to initiate the DDT. The pre-exponential factors are smaller than those anticipated in real fuel-oxidiser reactions, even if the largest value cited in Table 3 is used.

In the previous 1-D simulations found in [6, 8] a common figure used to compare different cases is the globally integrated heat release as a function of time. The global heat release is defined as the integral over the fluid volume V of the chemical heat release rate at each instant in time so that

$$\dot{Q}_{\mathrm{ch}}(t) = \int_V \dot{W}(t) q \, \mathrm{d}V. \tag{8}$$

Figure 1 shows the currently calculated global heat release transient for $E = 13.79$ in comparison with that in [8]. The two solutions are nearly identical, with the exception of the small local maximum that occurs when $27 < t < 30$ in [8] after the overdriven detonation is formed. That local maximum is attributed in [8] to the consumption of a localised pocket of unburned fuel still present after the detonation wave is formed.

Both solutions decay eventually to the theoretical steady-state heat release value of $\dot{Q}_{\mathrm{CJ}} = 83.14$. Although there are some minor quantitative differences between the two results, the concepts developed in [6] and [8] are observed to be independent of the applied numerical method.

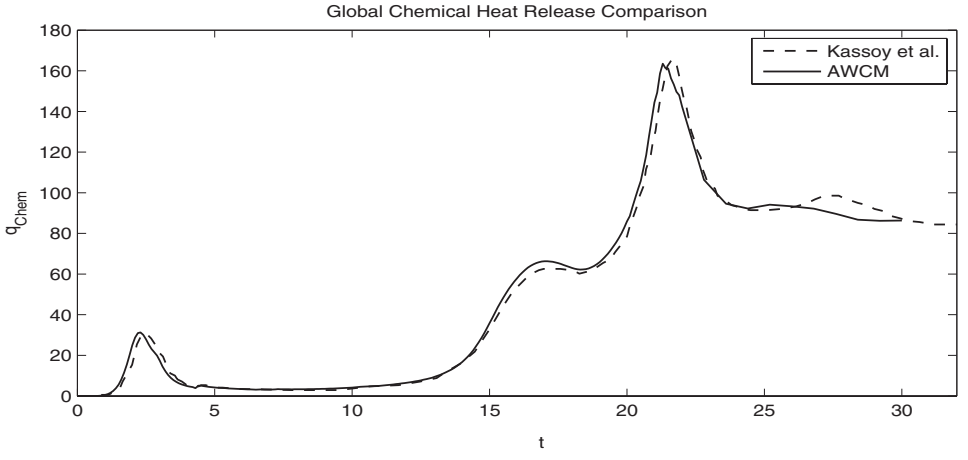

Figure 1. The global chemical heat release shows the initial ignition of the reactive fluid ($2 \leq t \leq 4$), the induction period ($5 \leq t \leq 13$) and the localised explosion ($15 \leq t \leq 18$) that releases the energy that creates an over-driven detonation wave that decays to a C–J wave. The Kassoy *et al.* results closely match the AWCM results leading to detonation formation.

4. Acoustic timescale theory

The evolution of detonation formation following localised acoustic timescale power deposition can be visualised on the x–t diagram schematically illustrated in Figure 2, which is constructed from previous work [6, 8] and detailed computational results presented in Section 5.2. The process includes localised thermal power deposition causing a shock wave to form and propagate away, an immediate exothermic rapid reaction on the acoustic timescale (explosion) that is the source of compression waves, an induction period within the reactive gas conditioned by the passage of shocks and compression waves, including shock reflection and transmission, a subsequent localised explosion that creates an accelerating reaction front, overdriven detonation wave formation, and relaxation to a steady-state detonation wave. This figure is very similar to others seen in [6, 21, 41]. Figure 2 focuses explicitly on the interaction between two individual explosions (dark grey field) in which the final explosion (right-hand boundary) intersects with the lead shock to produce an overdriven detonation wave. The results presented in Section 5.2 will show a more complex evolution process for cases with larger activation energies. Once the results are discussed, a modified diagram (Figure 8) will be proposed to explain the different evolution processes observed.

The process begins near the wall $x = 0$ at $t = 0$ with the initial thermal power deposition that creates a compression wave that transitions to a shock and propagates downstream. The shock wave heats the gas to a temperature T_{s1} labelled in the legend of Figure 2. When the reactants reach an adequately high temperature, a chemical explosion occurs inside the deposition region, which creates compression waves in both the positive and negative directions. Waves are commonly labelled using the symbol ψ. Figure 2 denotes the waves travelling in positive and negative directions as ψ_R and ψ_L, respectively. The ψ_R wave decouples from reaction zone and propagates toward the lead shock. At some point the ψ_R wave reaches the lead shock and the two waves coalesce into a single shock wave with a higher post-shock pressure and temperature. When the two waves coalesce a momentary increase in the reaction rate releases a small amount of heat, which forms a localised hot spot.

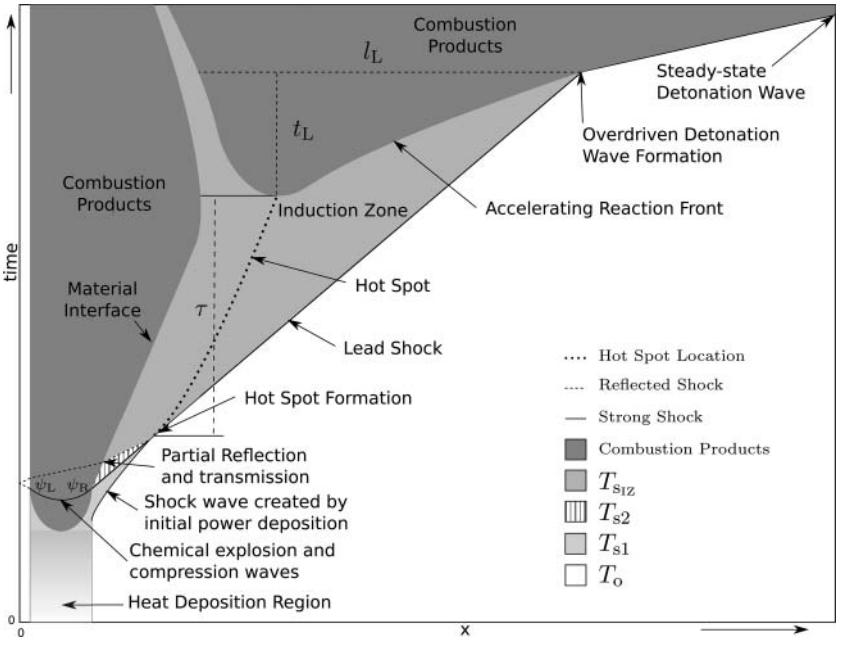

Figure 2. Generic x–t diagram demonstrating the process of power deposition, gasdynamic heating, localised reaction formation, accelerating reaction front, overdriven detonation wave formation and relaxation to steady-state detonation.

The material interface between the burned and unburned fluids acts as a partial reflection and transmission boundary for the ψ_L shock wave. Each time it reflects off the material interface its pressure ratio decreases because of the energy loss in transmission. The transmitted portion of the ψ_L branch wave coalesces with the lead shock and the lead post-shock temperature is increased. As with the ψ_R branch wave's coalescence with the lead shock, when the ψ_L branch wave intersects with the lead shock a momentary increase in the reaction rate releases a small amount of heat which forms a localised hot spot. Figure 2 shows the ψ_L and ψ_R branch waves reaching the lead shock simultaneously. This is rarely if ever the case, but this assumption is made to simplify the diagram. In previous work [6, 8] with low activation energies, even though the two hot spots are formed at different times, they explode nearly simultaneously, which is why a wide single hot spot is portrayed in the x–t diagram.

Figure 2 has been labelled to represent the different regions of temperature. The undisturbed reactants at T_o are coloured white, the combustion products are coloured dark grey, the induction zone created by the initial power deposition is denoted by T_{s1}, T_{s2} denotes the induction zone created by the ψ_R shock and $T_{s_{IZ}}$ denotes the final induction zone temperature created by the ψ_L branch wave. The post-shock temperature increases each time a new shock passes through the induction zone such that

$$T_0 < T_{s1} < T_{s2} < T_{s_{IZ}}. \tag{9}$$

This highly transient process creates an induction zone with a non-uniform induction time $\tau(x)$. The hot spots created by the subsequent shocks coalescing with the lead shock mark

the location of minimal induction time and are indicated in Figure 2 as black dots that move tangentially with the local fluid velocity.

After the induction zone's time τ has elapsed a localised explosion of nondimensional width l_{L} occurs in a period of time t_{L} as labelled in Figure 2. This explosion forms an accelerating reaction front that eventually reaches the lead shock and forms an overdriven detonation wave. The accelerating reaction front can be seen as the reduction in slope $\mathrm{d}t/\mathrm{d}x$ of the explosion's right boundary.

The nondimensional local acoustic timescale for this volume of fluid is defined as

$$t_{\mathrm{a_L}} = \frac{l_{\mathrm{L}}}{a_{\mathrm{L}}} = \frac{l_{\mathrm{L}}}{\sqrt{T_{\mathrm{L}}}}, \tag{10}$$

where the local nondimensional speed of sound is a function of the local fluid temperature: $a_{\mathrm{L}} = \sqrt{T_{\mathrm{L}}}$. Partial inertial confinement will occur when the chemical heat release time $t_{\mathrm{L}} \lesssim t_{\mathrm{a_L}}$ and total inertial confinement will occur in the limit $t_{\mathrm{L}} \ll t_{\mathrm{a_L}}$. It is convenient to define a local acoustic timescale ratio

$$r_{\mathrm{L}} = \frac{t_{\mathrm{L}}}{t_{\mathrm{a_L}}} \tag{11}$$

that can be used to characterise the results. When the local acoustic timescale ratio for a given hot spot is unity the pressure rise is limited by gas expansion simultaneous with the local heat release. Thus, timescale ratios less than unity should be associated with pronounced inertial confinement and significant local pressure enhancement that promotes the appearance of an accelerating reaction front that forms an overdriven detonation wave. Timescale ratios greater than unity are associated with significant gas expansion leading to a decelerating heat release process that eventually terminates.

5. DDT with large activation energies

As the activation energy is increased to values beyond that used in the benchmark simulation, the amount of time required to achieve a DDT increases as observed in [6] and [8]. This is readily explained by inverting Equation (3) to obtain a proportionality relationship between the characteristic reaction time t_{ch} and the activation energy E for a localised volume of fluid that has been compressed by a shock wave so that the post-shock temperature of the fluid is T_{s}:

$$t_{\mathrm{ch}} \propto e^{(E/T_{\mathrm{s}})}/B. \tag{12}$$

As the activation energy increases the time required for the preheated fluid to react increases exponentially. Kassoy *et al.* [8] observed this sensitive response to activation energy by reducing the activation energy from 13.79 to 12.50, which reduced the induction time by an amount similar in magnitude to the induction time itself. It is also observed that reducing the deposition amplitude increases the DDT time by reducing the post-shock induction zone temperature. In the 50% amplitude case, it was shown that the heat release profiles showed multiple inflection points in the globally integrated heat release rate. This change in heat release rate occurs because there is not one but two hot spots that are formed during the initial transients. Multiple inflection points arise in the heat release rate because the hot spots no longer react simultaneously. Thus, a reduction in the power deposition amplitude

not only reduces the induction zone temperatures, but also introduces a variation in the induction times for each hot spot.

Modification of the power deposition amplitudes by up to 50% show only minor variations in the induction periods of the two hot spots. Since the reaction rate is an exponential function of activation energy, it can be anticipated that an increase in activation energy may create substantial variations in induction periods for each hot spot and potentially lead to behaviour different from that seen in [6, 8].

One of the primary objectives of the present work is to investigate the effect of incremental increases in activation energy higher than 13.79 to determine if a similar staggered hot spot behaviour occurs. A second objective is to model a scenario that uses a moderately high activation energy and determine if the trends observed in the incremental study are consistent with that observed for the high activation energy case. The final objective is to characterise the thermomechanical behaviour of the observed hot spots in terms of localised length and acoustic timescales.

5.1. *Problem formulation*

Four different 1-D simulations are presented for the activation energies and pre-exponential factors given in Table 3. The simulations are identical to that in the validation problem in Section 3.1.1 and the theoretical discussion in Section 4. The initial conditions are for a reactive mixture at rest in a homogeneous thermodynamic state. Thermal power deposition occurs in the region $x \in [1, 5]$. Cases 1–3 focus on an incremental increase in activation energy while maintaining the same pre-exponential factor B. Case 3 uses a power deposition amplitude 20% higher than Cases 1 and 2. The discussion in Section 5.2.3 will explain why this modification does not adversely affect the conclusions drawn from the results. Case 4 uses an activation energy $E = 25$, a pre-exponential factor $B = 440$ and an increased amplitude $A = 2$. The change in pre-exponential factor and amplitude is necessary since the relatively high activation energy makes it difficult to predict a priori the computational domain size needed to capture detonation formation inside the domain. However, since Case 4 varies so significantly from the other cases it should be considered an example of

Table 3. Summary of parameters used for each case in 1-D simulations. The amplitude and power deposition duration have been modified for Cases 3 and 4 to ensure detonation initiation occurs within the computational domain while still depositing the same energy as in the previous two cases ($x_{\max}$ is the domain length, n_x is the maximum effective number of grid points, Δx is the finest grid spacing, $\Delta_{1/2}$ is the steady-state half-reaction length and $n_x/\Delta_{1/2}$ is the effective number of points to resolve the half-reaction length).

Case	1	2	3	4
ε^*	0.0750	0.0675	0.0650	0.0400
B	15	15	15	440
t_a	0.5	0.5	0.5	0.5
t_b	10	10	8.1	5.25
A	1	1	1.2	2
$x_{\max}$	150	150	300	60
n_x	7680	7680	15360	30720
Δx	0.0195	0.0195	0.0195	0.00195
$\Delta_{1/2}$	0.3808	0.4548	0.4868	0.0532
$n_x/\Delta_{1/2}$	19.5	23.3	24.9	27.2

what happens in the limit of large activation energies and not an incremental extension of Cases 1–3.

5.2. *Results*

Results for various simulations have been used to construct x–t diagrams as seen in Figures 3, 5, 6 and 7. The coloured contour portions provide results for some or all of the pressure, reaction rate, temperature and fuel mass fraction. In each x–t diagram the creation of a hot spot is demarcated by a closed white circle and is numbered in the order of appearance. Open black circles mark the time and location that the hot spots release the majority of their chemical energy in a rapid reaction after their induction period has elapsed. Red circles indicate locations where a reaction front intersects another shock wave.

Figure 4 plots the globally integrated chemical heat release defined in Equation (8) for each case. Each plot is labelled to indicate the creation of a hot spot, the spot's induction time τ and the heat release period for that localised explosion t_{L} as discussed in Section 4 and in Figure 2.

The black dots trace coordinates of the shock locator function ϕ described in Section 3 for values greater than 0.9. These dots are good indicators of local maxima and shocks. A value of 0.9 is chosen because at higher values the shocks become difficult to recognise and at lower values the dots become overly abundant and structures become difficult to distinguish from each other. The white arrows are used to represent the fluid velocity. A vertical arrow indicates zero velocity and a horizontal arrow would indicate an infinite velocity. Each of the examples depicts a sequence of events similar to that in Figure 2. Although the reactive gasdynamics becomes increasingly complex with increased activation energy the basic driving mechanism of localised chemical heat release is common to each simulation.

5.2.1. *Case 1: $E = 13.33$*

Figure 3 shows the x–t diagrams of (a) temperature, (b) fuel mass fraction, (c) pressure and (d) reaction rate for the simplest case with an activation energy $E = 13.33$. The simulation begins with energy deposited in the region $x \in [1, 5]$, heating the gases and creating a local rise in temperature and pressure. Two trails of black dots that start at $t = 0$ indicate shock waves that are created by the thermal power deposition. The right set propagates to the right away from the energy source and the left branch propagates to the left. At $t = 2$ the reactants inside of the deposition region are consumed in a rapid explosion producing left and right (ψ_{L} and ψ_{R}) compression waves. The right ψ_{R} compression wave coalesces with the lead shock created by the original thermal power deposition and creates localised hot spot 1. This hot spot is marked as a closed white circle in Figure 3. The ψ_{L} wave reflects off the left wall and travels back through the hot gas, the material interface that marks the boundary between the reacted and unreacted fluids and into the unreacted fluid. The black dots show the path of this shock starting at the left wall at $t = 3$. When the reflected ψ_{L} wave reaches the material interface at $t = 4.2$, the pressure contour indicates that part of this wave is reflected while the majority of it is transmitted. The initial post-shock temperature as described in Section 4 after the creation of the first hot spot is $T_{\mathrm{s1}} = 1.7$.

At $t = 4.2$ the transmission of the reflected ψ_{L} branch wave occurs and increases the post-shock temperature to $T_{\mathrm{s2}} = 2.2$. The transmitted ψ_{L} wave reaches the lead shock at $t = 6.5$. The second hot spot forms when the ψ_{L} transmitted wave coalesces with the lead shock at $t = 6.5$. Hot spot 2 is labelled in Figure 3(a) by a closed white circle.

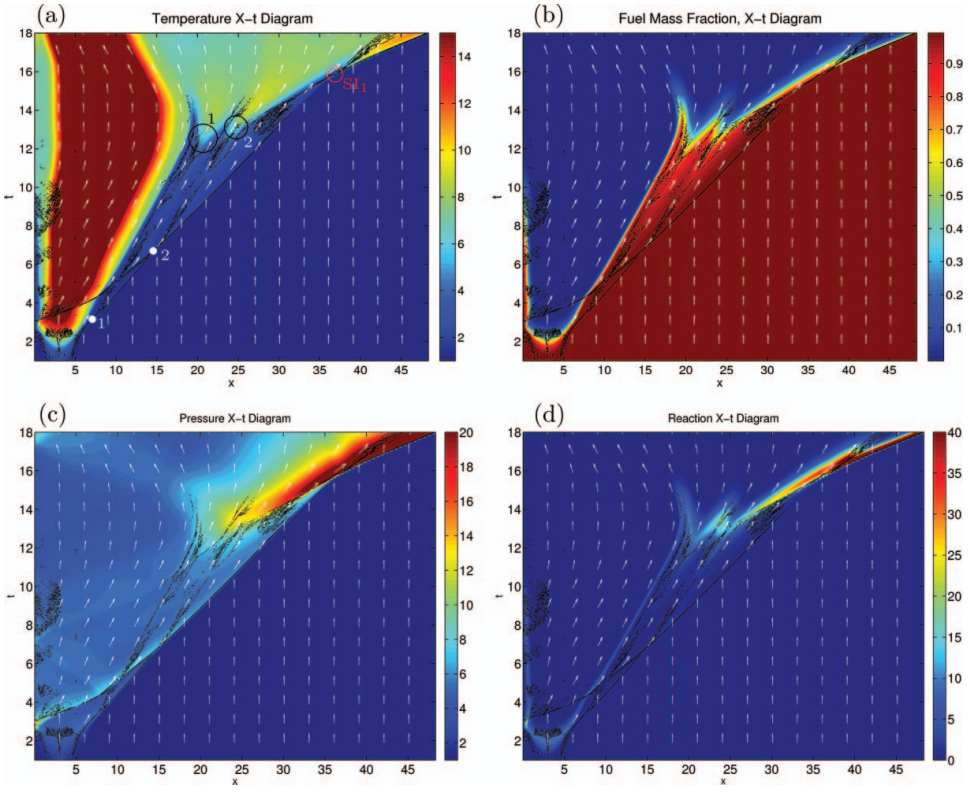

Figure 3. Case 1: x–t diagrams for (a) temperature, (b) fuel mass fraction, (c) pressure and (d) reaction rate are shown using $B = 15$ and $E = 13.33$. Black dots indicate areas of localised activity, *e.g.* shock waves and other localised structures. The white arrows indicate fluid velocity direction. This case contains two hot spots that react simultaneously and create an accelerating reaction front that ends when it reaches the lead shock at SI_1.

After hot spots 1 and 2 have been created, an induction period commences in which small amounts of chemical heat are released. Figure 4(a) labels the hot spot creation and induction times for the globally integrated heat release. Once the induction period has ended at $t = 12$ with an increase in heat release rate, Figure 3(d) shows that these hot spots simultaneously form two spontaneous explosions and consume all the reactants in the induction region. The event resembles a classic spontaneous explosion that can be characterised by concepts developed by Zeldovich [17] and co-authors and Lee [19], where each particle reacts according to its individual chemical induction time. Figure 3(d) also shows that the chemical heat release between $t = 12$ and $t = 14$ differs from that from $t = 14$ to $t = 15.6$. When $12 \leq t \leq 14$, the explosion begins. As discussed in Section 4, the final explosion includes an accelerating reaction front. This reaction front is seen in Figure 3 during the interval $14 \leq t \leq 15.6$. The slope of the reaction front, $\mathrm{d}t/\mathrm{d}x$, in that interval is approximately equal to the slope of the detonation wave for $t > 15.6$. Equal slopes indicate that the propagation speed $u_{\mathrm{sp}} = D_{\mathrm{CJ}}$, which suggests that a detonation wave will form.

Just before the reaction front reaches the lead shock front at $t = 15.6$ the gas temperature from the compression wave is $T \approx 4$. When the wave reaches the lead shock the local

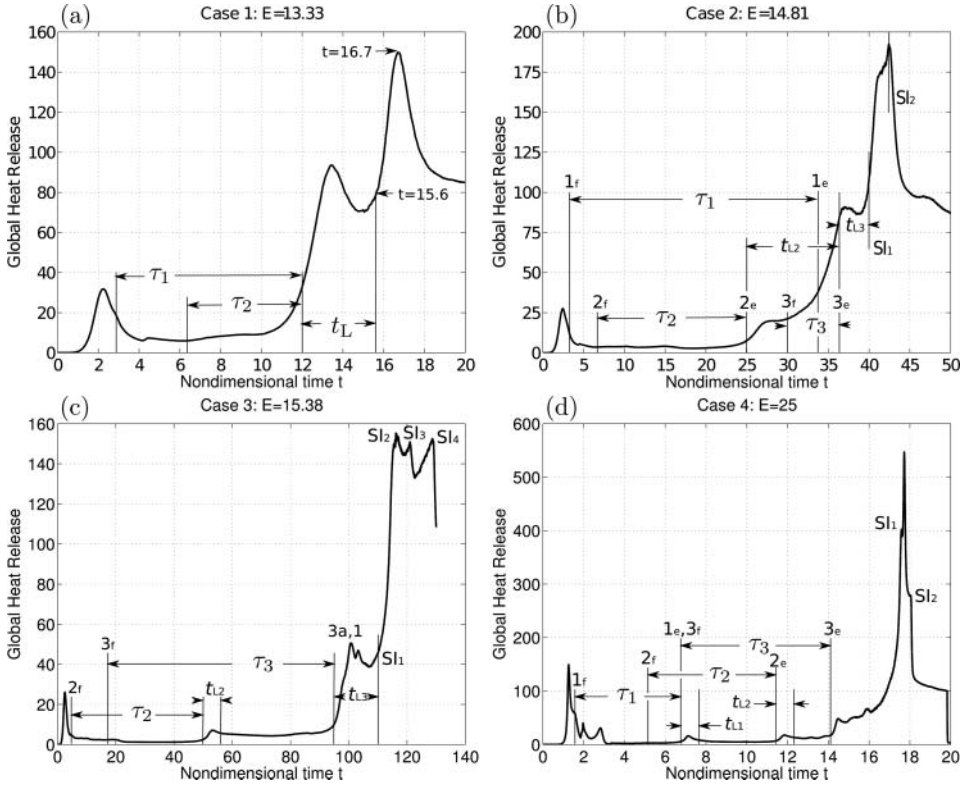

Figure 4. Global heat release plots for the four different cases. Each case shows multiple explosions leading to a final explosion that coincides with a compression wave entering a cooler fluid, which increases the acoustic timescale so that the reaction is more inertially confined and an overdriven detonation wave is created.

acoustic time equals the unreacted acoustic time. Once the reacting structure of substantial width is inside the unreacted gas the acoustic timescale increases by a factor of 2 (because $T \approx 4$) so that one final rapid chemical explosion takes place and consumes the remainder of the reactants located behind the shock leading to an overdriven detonation wave. This final explosion corresponds to the peak heat release rate at $t = 16.7$ in Figure 4(a), beyond which the global heat release decays to the steady-state CJ rate $\dot{Q}_{\mathrm{CJ}} = 83.2$.

5.2.2. *Case 2:* $E = 14.81$

In Case 2 the activation energy is increased to $E = 14.81$, 11% greater than Case 1, while the pre-exponential factor remains the same with $B = 15$. Figure 5 shows that the sequence of events begins similarly to that in Case 1, but quickly differs as time evolves. Two hot spots are formed in the same early transient process as in Case 1. However, their evolution into a detonation wave is distinctly different. This evolution includes the creation of an additional hot spot out of the explosion of one of the original hot spots.

Perhaps the most obvious difference is that the time required to create the detonation wave in the undisturbed reactive gas is increased from $t = 15.6$ to $t \approx 42$. With the increased activation energy the gas reacts more slowly to the initial power deposition, which

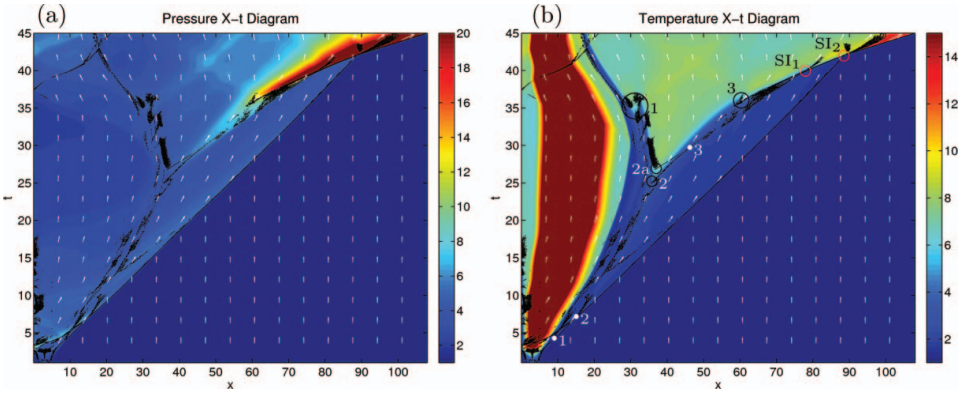

Figure 5. Case 2 x–t diagrams for (a) pressure and (b) temperature using $B = 15$ and $E = 14.81$. Two hot spots (1 and 2) form during the initial transients. The second hot spot explosion begins slowly and creates another reaction centre (3). When the reaction front from hot spot 2 intersects with hot spot 3 the third explosion occurs.

creates an initial explosion with smaller post-shock pressures than is seen in Figure 3 for Case 1. Lower shock pressures create lower post-shock temperatures and longer induction times for each hot spot.

Figure 4(b) plots the global heat release for Case 2 and labels the formation (subscript f) and explosion (subscript e) times for each hot spot. The hot spots are numbered in the order in which they are formed. The heat release profile shows that there is not one but two local peaks in heat release that occur after the initial explosion and prior to the global maximum.[2] Each heat release maximum is indicative of a separate explosion somewhere between the wall and the lead shock.

The inflection in heat release near $t = 25$ can be used to locate the first explosion that ignites hot spot 2. This explosion is labelled on the x–t diagram in Figure 5 at $x = 38$ and $t = 25$ with two black circles. Circle 2 marks the beginning of the explosion of hot spot 2 and highlights the origination of compression waves that emanate from it. Slightly after the beginning of explosion 2, circle 2a marks the rapid end of the explosion. Circle 2a captures the creation of compression waves that originate from this point. The compression waves that originate from point 2a travel at a faster speed than the waves originating from point 2, which causes them to coalesce to create hot spot 3. Figure 5 demonstrates the convergence of these two characteristic lines with black dotted lines that terminate at the white circle 3. The two waves coalesce into a single shock wave which propagates downstream until it intersects the emerging detonation wave at the point SI_1.

At $t \approx 35$, Figure 4(b) shows the induction times for both hot spots 1 and 3 to come to an end. Figure 5 shows that both explosions 1 and 3 occur at roughly the same time. The heat release maximum near $t = 35$ is likely to be formed from contributions of both hot spot's chemical heat release. However, it is only the heat release from hot spot 3 that plays a direct role in the detonation formation process. The explosion from hot spot 3 creates a strong shock wave with a slope substantially less than the shock created by explosion 2.

[2]Although the heat released in $25 < t < 30$ does not create a true maximum, it still acts as an indication of an explosion that has occurred. Thus it will be referred to as a maximum in the heat release.

The pressure associated with this shock wave exceeds 20 as indicated in Figure 5. The figure shows that the two shocks intersect at $x \approx 76$ and $t \approx 40$, marked by the red shock intersection circle SI_1. Just as in Case 1, when the two shocks intersect the fluid changes from one acoustic timescale to another, which creates a moment of partial inertial confinement and a rapid release of chemical energy occurs. The rapid increase of heat release shown in Figure 4(b) near $t = 40$ or SI_1 delineates this event.

What is distinctly different about this case from Case 1 is that the overdriven detonation wave is formed before reaching the undisturbed gas. Beyond this point the detonation propagates through the low-temperature fluid until it reaches the lead shock front at $t \approx 42.5$ or SI_2. The global maximum for the heat release plot in Figure 4(b) coincides with the detonation wave reaching the lead shock front. Although Case 1 and Case 2 share similar origins, the basic character of the global heat release differs dramatically from that in Figure 4(a).

5.2.3. *Case 3:* $E = 15.38$

The Case 3 activation energy is only 3.8% larger than that in Case 2 corresponding to $E = 15.38$. The pre-exponential factor remains at $B = 15$ as in Cases 1 and 2. In this case the amplitude of the power deposition has been enhanced from unity to 1.2. Figures 4(c) and 6 show that the induction time has increased so that the detonation in the unreacted gas does not form until $t \approx 128$.

Figure 6 shows that three hot spots form during the initial transient process. The first two occur in the same fashion as in the previous cases. Hot spot 3 is formed by a compression wave that is created by a localised explosion that occurs in the unburned reactants near the wall. The black dotted path the compression wave takes is not visible until it enters the unreacted fluid. Once the compression wave travels through the unreacted fluid and coalesces with the lead shock, hot spot 3 is created.

Three localised explosions occur after the initial power deposition and prior to detonation initiation. The first hot spot to react is hot spot 2 and is distinctly separate from explosion 3. Explosion 2 does not release heat fast enough to produce compression waves that can preheat the gas sufficiently to create an accelerating reaction front. This

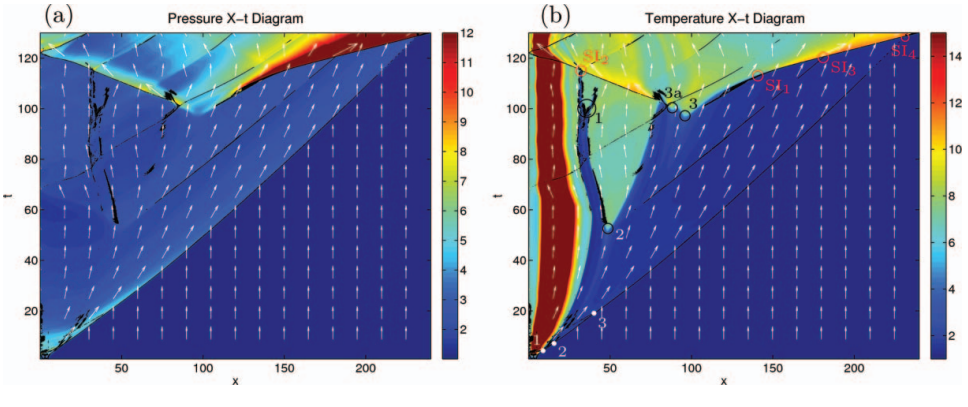

Figure 6. Case 3 x–t diagrams are shown for (a) pressure and (b) temperature with $B = 15$ and $E = 15.38$. Three recognizable hot spots are generated during the initial transients. Hot spot 2 is the first to react and reacts in two parts, 2 and 2a. Explosion 3 creates an accelerating reaction front that intersects its own created shock wave and the previous two shock waves created before it.

is evidenced in Figure 6(b) by observing that the slope of the interface between the reacted and unreacted gases increases instead of decreases. The global heat release plot in Figure 4(c) shows that the heat release at $t = 50$ does not create an accelerating reaction front characterised by an increasing heat release rate as seen in Figure 4(b) between $t = 27$ and $t = 37$ of the previous case. Instead, the hot spot reacts rapidly enough to generate compression waves, but the reaction is subsequently terminated, as indicated by the reduction in heat release rate. The figure shows that the global heat release rate of the reactive fluid has increased from a rather low value ~ 2 before the explosion of hot spot 2 to a value of 5 near $t = 60$. Although this explosion does not create an accelerating reaction front, it does increase the heating rate of the induction zone. What is remarkably different about explosion 2 in this case is that the time associated with the heat release time is easily identifiable with a distinguishable start and finish as indicated by the label t_{L2}. This is characterised by the relatively constant heat release both before and after the explosion, which indicates that the explosion did not remove the fluid from an induction state.

At $t = 95$ explosion 3 occurs after its induction period has ended. Figure 6(a) shows the creation of compression waves with pressures above 5 such that an accelerating reaction is created. The decreasing slope in Figure 6(b) as well as the increasing heat release rate in Figure 4(c) from $t = 95$ to $t = 100$ typifies the accelerating reaction wave. Shortly after the beginning of explosion 3, explosion 3a and explosion 1 release additional amounts of heat, as indicated by two maxima inside of the t_{L3} heat release region. At $x \approx 138$ and $t \approx 113$ (point SI_1) the accelerating reaction intersects the shock wave produced by hot spot 3's localised explosion and the acoustic timescale changes. As seen in the previous cases, when this occurs a rapid release of chemical energy occurs and is evidenced in Figure 4(c) by the sudden increase in heat release between $t = 110$ and $t = 115$ after SI_1. Once this occurs a detonation wave has formed and now propagates through two more shocked regions before entering the undisturbed fluid at $t \approx 128$.

5.2.4. *Case 4: $E = 25$*

Case 4 is distinctly different than the other cases because it is based on an activation energy $E = 25$ and a pre-exponential factor $B = 440$. These values are significantly different than the previous three cases and it should be considered as a limiting case of the type of behaviour that might be expected from a reactive fluid with a moderately high activation energy. The initial transient behaviour is similar to that in the previous cases. Here again hot spots are created during the initial transients, which then trigger localised explosions. However, the difference in parameters substantially alters the DDT time-frame and the number of localised explosions that occur prior to detonation formation.

Figure 7 demonstrates the pressure (a) and temperature (b) response to the initial explosion induced by the thermal power deposition. Three distinct hot spots are formed during the initial transient period. Hot spots 1 and 2 are formed from the same processes as in the previous cases, but are created in less time. Hot spot 3 is created from an explosion of the reactants located along the wall at $t = 3$. A black dot along the wall at $t = 3$ in the x–t diagram identifies this explosion location. The black lines tracing the compression wave's path are diffuse, but adequate enough to see that they lead to the formation of hot spot 3. These three hot spots explode sequentially with the third explosion creating the accelerating reaction front that leads to detonation formation. The pressure contours and black dots that highlight the shock paths look remarkably similar to figure 3 in [21]. Each successive explosion increases the induction zone temperature until an accelerating reaction wave is formed. Figure 4(d) quantifies this progression by showing the gradual increase

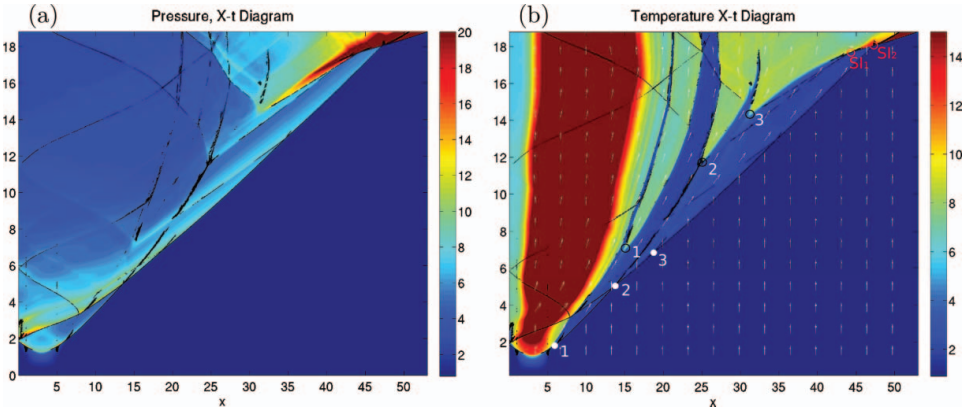

Figure 7. Case 4 x–t diagrams for pressure (a) and temperature (b) with $B = 440$ and $E = 25$. Three distinct hot spots are formed and react in successive order. Hot spot 3 creates an accelerating reaction front and the previous two do not.

in reaction rate with each successive explosion. At $t = 14$ the final explosion needed to facilitate the overdriven detonation wave occurs. The detonation forms at $t = 17.5$ while still in the shocked fluid and reaches the lead shock near $t = 18$. Figure 7 identifies the detonation formation with SI_1 and when the detonation reaches the lead shock with SI_2.

5.2.5. *Timescale analysis*

The local timescale ratio (Equation 11) can be used to explain how each localised hot spot affects the entire DDT process. If the ratio is less than unity (heating times less than the local acoustic time) the thermomechanical response is characterised by near inertial confinement [26] with the local pressure rising with temperature. The reactant is consumed on a timescale during which the low Mach number of induced motion implies that the fluid moves only a small fraction of the spot size. That fluid expelled from the hot spot acts as a piston, driving gasdynamic waves into the environment. If the ratio is greater than unity there is sufficient time for relative pressure equalisation to occur during the heat release period [26], which limits the maximum rise in local pressure. In this case the piston effect associated with expelled gas is smaller and the induced gasdynamic disturbances are weaker. Thus, if the ratio is less than unity an accelerating reaction front will be driven by relatively strong gasdynamic disturbances arising from the thermomechanical response of the hot spot and a subsequent detonation will appear.

Table 4 contains the local timescale ratios r_L for each hot spot in the four cases. The data presented in the previous sections suggests that there are two different types of hot spots. There are ‘strong’ hot spots that create an accelerating reaction front and there are ‘weak’ hot spots that release their chemical heat and produce a shock wave, but no accelerating reaction front is created. The x–t diagram in Figure 2 is an example of a strong hot spot and does not depict the behaviour of a weak hot spot. Figure 8 shows an x–t diagram for a weak hot spot. In both diagrams, the local explosion time t_L and length l_L are labelled. For the strong hot spot, the explosion time is defined as the time from which the rapid explosion begins to when it is interrupted by an external process such as another shock. In the case of the weak hot spot, the explosion time is determined by looking at the global chemical heat release in Figure 4 and noting when the chemical heat release of the hot spot

Table 4. Table containing the local timescale ratios for Cases 1–4 and the values used in the calculations. The start and end times correspond to the times that each hot spot begins and ends its rapid chemical explosion. The left and right boundaries define the length scale associated with the hot spot explosion. This is taken as the width of the reacted hot spot at the finish time. The explosion times and lengths are labelled in Figure 2.

	Case							
	1	2		3		4		
Hot spot number	1	2	3	2	3	1	2	3
Start time, t_{sL}	12	25	36	50	95	6.50	11.4	14.0
End time, t_{eL}	15.6	36	40	56.3	122	7.6	12.4	17.5
$t_L = t_{eL} - t_{sL}$	3.6	11	4	6.3	27	1.1	0.91	3.50
Left boundary, x_L	18	32	60	46.6	80	15.4	25.1	32.0
Right boundary, x_R	38	60	78	55.7	180	16.3	26.2	44.0
$l_L = x_R - x_L$	20	28	18	9.1	100	0.875	1.1	12.0
Induction temperature, T_L	2.2	1.85	2.2	1.8	1.85		2.45	
Acoustic timescale, t_{aL}	13.48	20.6	12.1	6.78	73.5	0.56	0.72	7.67
Weak (W) / Strong (S)	S	S	S	W	S	W	W	S
Timescale ratio, $r_L = t_L/t_{aL}$	0.27	0.53	0.33	0.92	0.37	2.03	1.26	0.46

has terminated. Weak hot spots are characterised by a distinct small localised maximum in heat release following the end of the induction period. The localised heat release time t_L is labelled for each hot spot in each of the four cases considered with one exception.[3] The characteristic length associated with a weak hot spot's localised explosion is defined as the width of the burned fluid at the end of the heat release time t_L. The widths are retrieved from Figures 3, 5, 6 and 7. Table 4 has tabulated the start and end times as well as the left (x_L) and right (x_R) boundaries of each explosion in addition to the actual length and timescales. It contains the local induction zone temperatures, acoustic timescales, whether the hot spots form weak or strong explosions and the timescale ratios for each hot spot that plays a role in detonation formation.

Prior to the discussion of the results, several remarks should be made about the timescale ratios. First, the temperature used to determine the local timescale is evaluated at the time the hot spot is created. When each of the hot spots are first formed the hot spot temperature is about 10% higher than the rest of the induction zone. Remarkably, gradual chemical heating causes the average spatial temperature inside the induction zone to be approximately equal to the initial temperatures listed in Table 4. However, just before explosion, the temperature variation can be as high as 50% of the mean. For example, at $t = 85$ the average induction zone temperature for hot spot 1 in Case 3 is 1.8, while the minimum and maximum temperatures vary from 1.4 to 2.1. With this range of values, the local timescale ratio of hot spot 1 in Case 3 can range from 1.0 at the hot spot peak to 0.81 far from the hot spot centre. It should also be noted that hot spot 2 in Case 2 is treated as a strong hot spot, even though it does not directly lead to a detonation wave, because Figure 4(b) shows that the explosion period for hot spot 2 contains an increasing heat release, which typifies an accelerating reaction front. The accelerating reaction front for this hot spot is represented on the x–t diagram (Figure 5) by the decrease in slope of the material interface following

[3]The heat release time for hot spot 3 in Case 4 is not explicitly labelled, but it is to be understood as the time the induction period ends until the first shock interaction at SI_1.

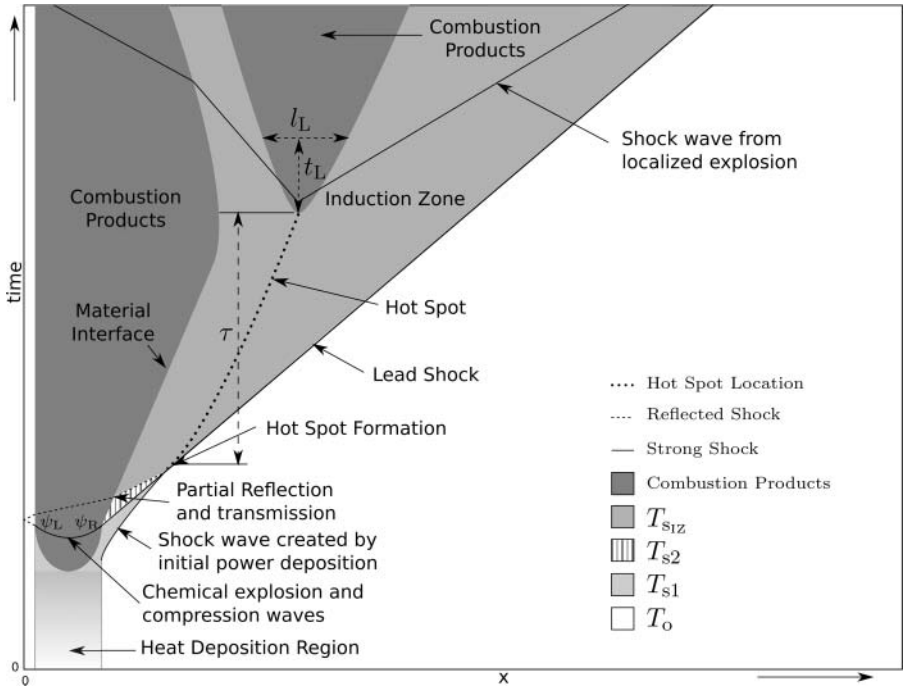

Figure 8. Generic x–t diagram for the creation of a hot spot that produces a shock wave, but does not create an accelerating reaction front. The localised heat release time t_L is defined as the time it takes for the majority of the chemical energy contained inside the hot spot to be released in a rapid explosion creating a local maximum in the global heat release. The length scale is defined using the width of the burned hot spot after the heat release is finished.

explosion 2. The primary reason hot spot 2 does not directly form a detonation is because it is interrupted by the explosion from hot spot 3.

5.3. *Discussion on large activation energies*

The results from the previous sections indicate that as the activation energy increases and other parameters are fixed, the time required to form a detonation increases – see Figures 4(a)–(c). This expected result is consistent with those in [8] where the activation energy was varied over a small range of values (13.79, 13.33, 12.90 and 12.50). The results showed that the overall structure of the global heat release remained consistent over the observed range with a single localised maximum in heat release prior to the global maximum. Over that range of values, there was no appearance of additional localised inflection points or maxima because the two hot spots explode nearly simultaneously.

In the present work, the results indicate that as the activation energy increases, a variance in the induction times of each hot spot is introduced and the DDT heat release process becomes more staggered in time. This phenomena was first observed in [8] when the power deposition amplitude was decreased to 50%. This behaviour is characterised by the multiple inflection points and local maxima in the heat release rate prior to the global maximum. For convenience, the data for the 100% and 50% cases has been replotted in Figure 9. The reduction in the original chemical explosion volume temperature causes a

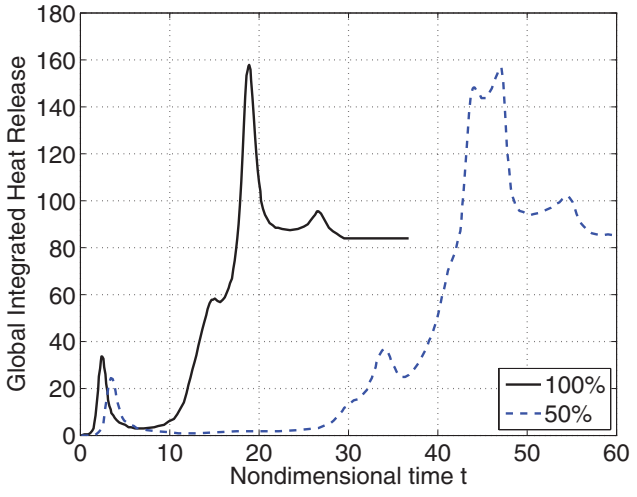

Figure 9. Global heat release rates from figure 15 in [8] for the full and half amplitude cases demonstrate a clear difference in the global heat release behaviour between the two cases. The multiple inflection points and localised maxima prior to the global maximum for the 50% magnitude case indicates the hot spots created during the initial transients react at different times during the DDT evolution process.

variation in induction times between the two hot spots, leading to multiple inflection points. These multiple inflection points and localised maxima in the heat release are a part of an overall increase in heat release rate characterised by an accelerating reaction front.

In Case 1 of the current work with $E = 13.33$, the activation energy is still within the range of activation energies used in [8]. The global heat release in Figure 4(a) contains a smooth transition from the original chemical explosion to the subsequent peak in heat release associated with hot spots 1 and 2. This characteristic behaviour is synonymous with the full power behaviour observed in [8].

Case 2 is based on an increased activation energy $E = 14.81$. The global heat release profile seen in Figure 4(b) shows a longer induction period followed by a sudden rise in heat release and then the heat release continues to rise until it reaches a local maximum. The sudden rise in heat release is caused by the explosion of hot spot 2 and the local maximum is created from the explosions of both hot spots 1 and 3. Explosions 2 and 3 are both considered strong hot spot explosions because of the accelerating reaction fronts created by each of them.

Figure 4(c) shows for Case 3 that, for just a 4% increase in activation energy above Case 2, the DDT time nearly triples. This trend is consistent with the results in [8], but there is a distinct change in behaviour not observed in any of the previous cases. The small increase in activation energy causes hot spot 2 to transition from a strong hot spot to a weak hot spot. The heat release profile demonstrates that after the explosion time t_{L2} of hot spot 2 has finished, the reactive gas is still in an induction state. In this case, hot spot 3 is the only hot spot that facilitates an accelerating reaction front.

Recall that Case 3 amplifies the power deposition amplitude by 20% to force the detonation to form inside the computational domain. An increase in amplitude will create a more rapid explosion and increase the induction zone temperature. This means that an increase in amplitude will inhibit hot spot 2's transition from the strong to the weak form.

Although, the change in amplitude may shorten the induction period, it does not play a role in the transition of hot spot 2 from strong to weak. This transition is purely a consequence of increased activation energy.

Case 4 differs significantly from the previous cases because it uses an activation energy $E = 25$, a pre-exponential factor $B = 440$ and a power deposition amplitude $A = 2$. Three distinct hot spots are formed in this case. Hot spots 1 and 2 are weak hot spots as demonstrated by the fact that the fluid remains in an induction state after they have released their chemical heat. It is hot spot 3 that facilitates an accelerating reaction front and ultimately a detonation wave.

The results presented in [6, 8] are based on activation energies small enough to ensure that the induction times for each of the hot spots created are nearly identical. This causes the hot spots to explode simultaneously and the globally integrated heat release to contain a single local maximum when both explosions occur. This explosion ensemble facilitates an accelerating reaction front that leads to an overdriven detonation wave. The current results show that as the activation energy increases the induction periods vary enough to create multiple inflection points and local maxima in the heat release while still creating an accelerating reaction front. At some transitional activation energy, the hot spots transition from strong to weak and their explosions no longer form an accelerating reaction front. It is essential to recognise that the localised thermomechanical response of the heated gas as described in [24] is the immediate source of the gasdynamic waves responsible for DDT evolution rather than the heat release itself.

The transition between weak and strong hot spots can be characterised in terms of the acoustic timescale theory developed in Section 4 and the timescale analysis performed in Section 5.2.5. The concept behind the timescale ratio is that, if the ratio is near unity, the fuel in the hot spot is consumed on a timescale similar to that on which pressure relaxation occurs (near inertial confinement cannot occur). In contrast, timescale ratios that are less than unity are associated with fluid volume fuel consumption on a timescale that does not permit pressure relaxation to occur (near inertial confinement). Ratios greater than unity are associated with extensive pressure relaxation concurrent with chemical heat addition. Thus, the local timescale ratio can be used to identify the transition between a runaway accelerating explosion and an explosion that terminates after being consumed. A weak hot spot is characterised by a minimal thermomechnical response (limited pressure rise and induced fluid motion amplitude) and a strong hot spot is characterised by a much stronger thermomechanical response, including gasdynamic wave generation that facilitates an accelerating reaction front. Table 4 lists the hot spots for each case, whether they create weak or strong explosions and the local timescale ratio for each hot spot. For each strong hot spot, the timescale ratio r_{L} is substantially less than unity. The timescale ratios for each weak hot spot are usually close to unity or greater. The one exception is the weak hot spot in Case 3, but as discussed in Section 5.2.5, this hot spot was classified as strong in Case 2. In Case 2 this hot spot's timescale ratio is $r_{\mathrm{L}2} = 0.53$, whereas in Case 3 the timescale ratio is increased to $r_{\mathrm{L}2} = 0.92$. The minute increase in activation energy reduces the induction zone temperature such that the hot spot's explosion timescale ratio is near unity and the fuel in the hot spot is consumed on a timescale similar to that on which pressure relaxation occurs. Thus the hot spot does not experience the inertial confinement required to facilitate an accelerating reaction front.

Each of the cases presented show a successful DDT process. With the exception of hot spot 3 in Case 2, each of the hot spots that play a role in achieving DDT are created during the initial transients. The analysis thus far has been predicated on at least the final hot spot exploding in a strong form. It is unclear whether a detonation will form if the final hot spot

to explode reacts in a weak form and terminates without creating an accelerating reaction front. The cases presented here focus on hot spots with timescale ratios near unity. In order to determine what happens for hot spots with higher timescale ratios where the final hot spot terminates, simulations must be done on significantly larger domains for extended periods of time.

6. Conclusions

The five objectives stated in the introduction have been achieved. The AWCM is shown to be a useful tool for resolving multi-scale compressible reacting flows. A replica of a problem addressed previously by Kassoy *et al.* [8] is solved using the AWCM. The results show that concepts developed in the previous work [6, 8] are independent of the applied numerical method. The results presented in this work confirm the qualitative conceptual ideas developed in earlier work and explain the concepts more quantitatively using x–t diagrams and timescale analysis.

The sensitivity of the DDT evolutionary process to small increases in activation energy is demonstrated by performing four different simulations. As the activation energy increases the multi-scale nature of the DDT evolutionary process, missing from the previous work, is demonstrated through the appearance of multiple peaks in the heat release rate. Although increased activation energy and decreased power deposition rates both show trends towards more temporally distributed heat release, it is the increased activation energy that reveals the truly multi-scale nature of the DDT process.

The importance of inertial confinement is demonstrated when the activation energy is increased such that, at some transitional activation energy, hot spots that facilitate an accelerating reaction front at lower activation energies cannot sustain an accelerating reaction front at higher activation energies. A distinction is made between the two different types of hot spot explosions, classified as weak and strong. Strong hot spots undergo an induction period and rapidly react creating compression waves that propagate away from the reaction source and facilitate an accelerating reaction front that eventually leads to detonation formation. These are the same types of explosions seen in previous work [6, 8]. Weak hot spots follow the same process, but terminate once the reactants are consumed. These weak hot spots have not been observed in the previous simulations [6, 8] because of the low activation energies used.

The distinction between weak and strong explosions is quantified by defining an acoustic timescale ratio associated with each hot spot explosion. A timescale ratio is defined as the ratio of the explosion heat release timescale to the local hot spot acoustic timescale. A strong hot spot explosion is characterised by a ratio less than unity and a weak hot spot explosion has a ratio near or greater than unity. These two types of hot spots are related to the work contained in [26] where the rate of heat addition into an inert gas determines the relative strength of a 'fluid piston' arising from localised gas expansion that drives gasdynamic waves into the surrounding fluid. The theory in [26] demonstrates quantitatively for an inert gas that when the localised energy addition is sufficiently limited for a given heating timescale, the induced Mach number of expansion is quite subsonic and only weak acoustic disturbances propagate into the neighbouring unheated gas. Alternatively, larger levels of energy deposition lead to much larger induced Mach numbers of expansion and more significant gasdynamic wave generation. In particular, the heating timescale and the energy addition are used to quantify the thermomechanical response of a locally heated hot spot. The stated conceptual perspectives are likely to pertain to reactive gases in which hot spots are generated by chemical heat release. Thus, it is possible that a more rigorous concept,

similar to that for inert gases in [26], may be developed for reactive gases that improves upon the timescale ratio presented here.

Acknowledgements

JDR appreciates the guidance and support of OVV and DRK during his PhD thesis research project. Support for this work was provided by the National Science Foundation (NSF) under grants No. ACI-0242457 and No. CBET-0756046. DRK acknowledges support from Air Force STTR contact FA955010C0088 for the thermomechanical aspects of the current work.

References

[1] J.F. Clarke, D.R. Kassoy, and N. Riley, *On the direct initiation of a plane detonation wave*, Proc. R. Soc. Lond. A 408 (1986), pp. 129–148.
[2] J.F. Clarke, D. Kassoy, N. Meharzi, N. Riley, and R. Vasantha, *On the evolution of plane detonations*, Proc. R. Soc. Lond. A 429 (1990), pp. 259–283.
[3] K. Mazaheri, *Mechanism of the onset of detonation in direct initiation*, Ph.D. diss., Department of Mechanical Engineering, McGill University, Montreal, Canada, 1997.
[4] C.A. Eckett, J.J. Quirk, and J.E. Shepherd, *An analytical model for direct initiation of gaseous detonation waves*, in *21st International Symposium on Shock Waves*, 20–25 July 1997, Great Keppel Island, Queensland, Australia, Paper 2100, Panther Publishing, Fyshwick, Australia.
[5] C.A. Eckett, J.J. Quirk, and J.E. Shepherd, *The role of unsteadiness in direct initiation of gaseous detonations*, J. Fluid Mech. 421 (2000), pp. 147–183.
[6] A.A. Sileem, D.R. Kassoy, and A.K. Hayashi, *Thermally initiated detonation through deflagration to detonation transition*, Proc. R. Soc. Lond. A 435 (1991), pp. 459–482.
[7] D.R. Kassoy, J.A. Kuehn, M.W. Nabity, and J.F. Clarke, *Modeling detonation initiation on the microsecond time scale*, in *Proceedings of the 43rd Aerospace Science Meeting and Exhibit*, 10–13 January 2005, Reno, NV, Paper 1169, AIAA.
[8] D.R. Kassoy, J.A. Kuehn, M.W. Nabity, and J.F. Clarke, *Detonation initiation on the microsecond time scale: DDTs*, Combust. Theory Model. 12 (2008), pp. 1009–1047.
[9] X. Gu, D. Emerson, and D. Bradely, *Modes of reaction front propagation from hot spots*, Combust. Flame 133 (2003), pp. 63–74.
[10] A. Khokhlov, E. Oran, and J. Wheeler, Combust. Flame 108 (1997), pp. 503–517.
[11] C. Montgomery, A. Khokhlov, E. Oran, and J. Wheeler, Combust. Flame 115 (1998), pp. 38–50.
[12] E.S. Oran and A.M. Khokhlov, *Deflagrations, hot spots, and the transition to detonation*, Phil. Trans. Roy. Soc. London Ser. A 357 (1999), pp. 3539–3551.
[13] A.M. Khokhlov, E. Oran, and G. Thomas, *Numerical simulation of deflagration-to-detonation transition: the role of shock–flame interactions in turbulent flames*, Combust. Flame 117 (1999), pp. 323–339.
[14] A.M. Khokhlov and E. Oran, *Numerical simulation of detonation initiation in a flame brush: the role of hot spots*, Combust. Flame 119 (1999), pp. 400–416.
[15] E.S. Oran and V.N. Gamezo, *Origins of the deflagration-to-detonation transition in gas-phase combustion*, Combust. Flame 148 (2007), pp. 4–47.
[16] A.K. Oppenheim, *Introduction to Gasdynamics of Explosions*, Springer-Verlag, New York, 1970.
[17] Y. Zeldovich, V. Librovich, G. Makhviladze, and G. Sivashinsky, *Development of detonation in a non-uniformly preheated gas*, Astronaut. Acta 15 (1970), pp. 313–321.
[18] Y.B. Zeldovich, *Regime classification of an exothermic reaction with nonuniform initial conditions*, Combust. Flame 39 (1980), pp. 211–214.
[19] J. Lee, R. Knustautas, and N. Yoshikawa, *Photochemical initiation of gaseous detonations*, Astronaut. Acta 5 (1978), pp. 971–982.
[20] L. Bauwens, *Ignition between a shock and a contact surface: influence of the downstream temperature*, Proc. Combust. Inst. 28 (2000), pp. 653–661.
[21] L. Bauwens and Z. Liang, *Shock formation ahead of hot spots*, Proc. Combust. Inst. 29 (2002), pp. 2795–2802.
[22] T.L. Jackson, A.K. Kapila, and D.S. Stewart, *Evolution of a reaction center in an explosive material*, SIAM J. Appl. Math. 49 (1989), pp. 452–458.

[23] M. Short, *The initiation of detonation from general non-uniformly distributed initial conditions*, Phil. Trans. R. Soc. Lond. A 353 (1995), pp. 173–203.
[24] M. Short, *On the critical conditions for the initiation of a detonation in a nonuniformly perturbed reactive fluid*, SIAM J. Appl. Math. 57 (1997), pp. 1242–1280.
[25] C. Vasquez-Espi and A. Linan, *Fast, non-diffusive ignition of a gaseous reacting mixture subject to a point energy source*, Combust. Theory Model. 5 (2001), pp. 485–498.
[26] D.R. Kassoy, *The response of a compressible gas to extremely rapid transient, spatially resolved energy addition: an asymptotic formulation*, J. Engrg. Math. 68 (2010), pp. 249–262.
[27] R. Sankaran, H.G. Im, E.R. Hawkes, and J.H. Chen, *The effects of non-uniform temperature distribution on the ignition of a lean homogeneous hydrogen–air mixture*, Proc. Combust. Inst. 30 (2005), pp. 875–882.
[28] A. Oppenheim and P. Urtiew, *Experimental observations of the transition to detonation in an explosive gas*, Proc. Roy. Soc. A 295 (1966), pp. 13–28.
[29] M.I. Radulescu, G. Sharpe, C. Law, and J. Lee, *The hydrodynamic structure of unstable cellular detonations*, J. Fluid Mech. 580 (2007), pp. 31–81.
[30] G.J. Sharpe and S.A.E.G. Falle, *Numerical simulations of pulsating detonations – I: Nonlinear stability of steady detonations*, Combust. Theory Model. 4 (2000), pp. 557–574.
[31] G.J. Sharpe, *Transverse waves in numerical simulations of cellular detonations*, J. Fluid Mech. 447 (2001), pp. 31–51.
[32] N.K.R. Kevlahan and O.V. Vasilyev, *An adaptive wavelet collocation method for fluid–structure interaction*, SIAM J. Sci. Comput. 26 (2005), pp. 1894–1915.
[33] O.V. Vasilyev, *Solving multi-dimensional evolution problems with localized structures using second generation wavelets*, Int. J. Comput. Fluid Dyn. 17 (Special Issue on High-resolution Methods in Computational Fluid Dynamics) (2003), pp. 151–168.
[34] O.V. Vasilyev and C. Bowman, *Second generation wavelet collocation method for the solution of partial differential equations*, J. Comput. Phys. 165 (2000), pp. 660–693.
[35] J.D. Regele and O.V. Vasilyev, *An adaptive wavelet-collocation method for shock computations*, Int. J. Comput. Fluid Dyn. 23 (2009), pp. 503–518.
[36] J.D. Regele, *Numerical modeling of acoustic timescale detonation initation using the adaptive wavelet-collocation method*, Ph.D. diss., University of Colorado, Boulder, CO, 2008.
[37] J.D. Regele, D.R. Kassoy, and O.V. Vasilyev, *Acoustic timescale detonation initiation in 2-D and its relationship with the 1-D description*, in *Proceedings of the 23rd International Conference on the Dynamics of Explosions and Reactive Systems (ICDERS)*, 24–29 July 2011, Irvine, CA.
[38] I. Glassman, *Combustion*, Vol. 3, Academic Press, 1996.
[39] R.A. Strehlow, *Combustion Fundamentals*, McGraw-Hill, 1984.
[40] S.R. Turns, *Introduction to Combustion – Concepts and Applications*, Vol. 2, McGraw-Hill, 2000.
[41] A.K. Oppenheim and H.G. Wagner, *Recent progress in detonation research*, AIAA J. 1 (1963), pp. 2243–2252.

Appendix A. Steady-state ZND propagation

It is important when employing a new numerical technique to a compressible reacting flow to verify that the numerical algorithm can correctly capture the detonation propagation velocity. In order to do this, an exact solution for the ZND model is found using [39] and is used as the initial condition for the AWCM solver. The solution is developed for a detonation wave moving with a Mach number $M = 5$ relative to the unburnt gas. The nondimensional heat of reaction q is related to the Mach number M by

$$q = \frac{1}{2}\frac{(M^2-1)^2}{(\gamma^2-1)M^2} \tag{A1}$$

so that the heat of reaction $q = 12$ with a specific heat ratio $\gamma = 1.4$. The activation energy $E = 10$ and pre-exponential factor $B = 5$. The jump conditions across the shock are found

Table A1. Each ZND case is listed with the total number of points n_x, their number of points per half-reaction length $n_x/\Delta_{1/2}$ and the peak post-shock density.

Case	n_x	$n_x/\Delta_{1/2}$	ρ_{max}
1	1000	22	4.354
2	2000	45	4.624
3	4000	90	4.795
4	8000	180	4.892

using the Rankine–Hugoniot relation giving the pre- and post-shock conditions

$$\begin{aligned} \rho_o &= 1 \qquad \rho_s = 5 \\ u_o &= 0 \qquad u_s = \sqrt{\gamma} \\ p_o &= 1 \qquad p_s = 29. \end{aligned} \tag{A2}$$

A single ODE for the fuel mass fraction is solved as a function of space downstream of the post-shock condition in order to determine the other dependent flow variables. It is verified that the flow satisfies the Chapman–Jouget conditions after combustion is complete with $p_{CJ} = 15$, $\rho_{CJ} = 5/3$ and $M = 1.0$. The ZND solution is solved in a domain $x \in [0, 20]$ with the shock located at $x = 20$. The computational domain used for the benchmark problem doubles the size of this domain so that $x \in [0, 40]$ with the initial shock location at $x = 20$. The solution is evolved until $t = 1.5$ so that the wave propagates approximately 40% of the computational domain. The exact solution is translated using the time t and the theoretical propagation velocity for comparison with the numerical solution. The simulation is performed with four different levels of resolution: 1000, 2000, 4000 and 8000 grid points. The half-reaction length for this simulation is 0.9, which, as discussed below, is important for assessing the level of resolution required for properly resolving the von Neumann spike.

Table A1 summarises the four different cases with their resolution (n_x), the number of points per half-reaction length and the corresponding maximum post-shock density. Figure A1 shows the comparison between the exact and numerical simulations for the detonation wave after a time $t = 1.5$ has elapsed. There is little noticeable difference in the shock's location for the numerical and exact solutions, which indicates that the numerical detonation velocity matches the theoretical velocity. Hence, the primary objective of this benchmark problem has been achieved.

Figure A1 shows that with the exception of the density there is little difference in post-shock conditions for most of the variables. For Case 1 the post-shock density is 12.9% below its theoretical value of 5 as noted in Equation (A2). The resolution in this case uses 22 points per half-reaction length, which is not adequate to capture the peak post-shock density fully. As shown in Table A1 and in Figure A2, the density maximum approaches the theoretical value of 5 as resolution is increased. Even though the post-shock peak amplitudes vary with resolution, the results confirm that the detonation velocity is independent of the numerical resolution. The slight fluctuations located at $x = 20$ and 26 in the solution profiles are standard initialisation errors that occur as a result of the initial transients encountered when starting the simulation with a discontinuous initial condition.

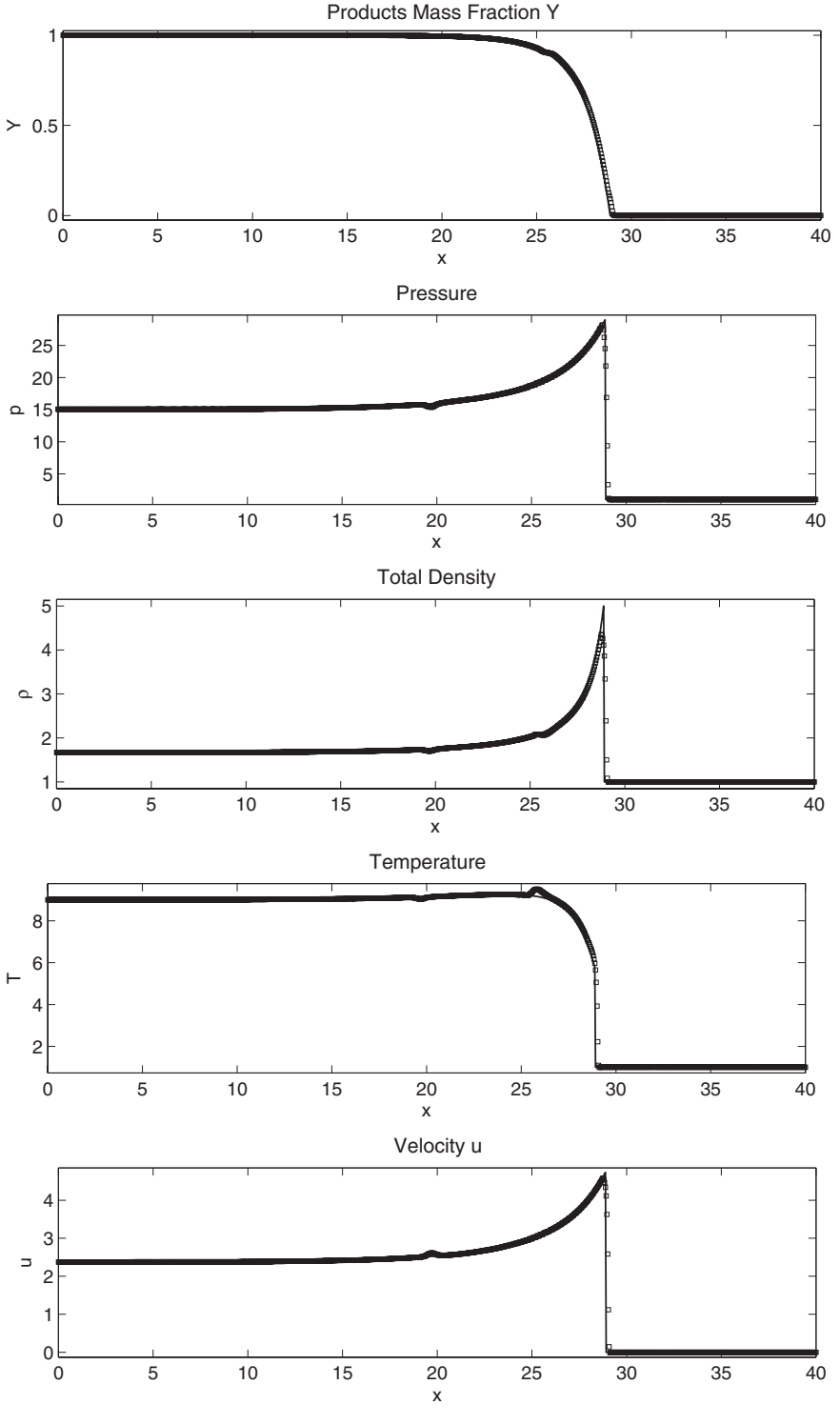

Figure A1. Comparison between the exact ZND solution and the Case 1 numerical solution after a time of $t = 1.5$ has elapsed. The solid lines and squares represent the exact and numerical solutions, respectively.

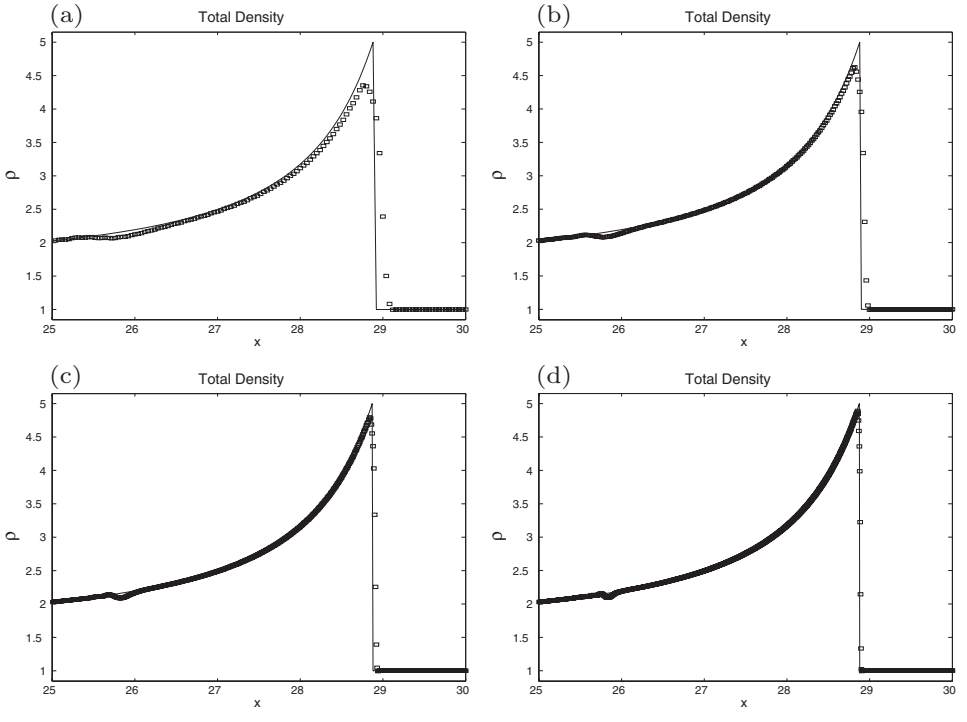

Figure A2. A close-up view of the density at $t = 1.5$ comparing the numerical solution with the exact solution for $n_x/\Delta_{1/2}$ equal to (a) 22, (b) 45, (c) 90 and (d) 180. Although the post-shock density deviation decreases and the shock width decreases with increased resolution, the detonation velocity stays constant.